fects, such as elastic waves in the gel (microsound) and local heating.

REFERENCES AND NOTES

1. See J. Maddox [*Nature* **345**, 381 (1990)] and A. Khurana [*Phys. Today* **240** (no. 8), 20 (1990)] for popular accounts of theoretical developments.
2. B. Norden, C. Elvingson, M. Jonsson, B. Akerman, *Q. Rev. Biophys.* **24**, 103 (1991).
3. J. L. Viovy, T. Dyke, F. Caron, *Contemp. Phys.* **33**, 25 (1992).
4. B. H. Zimm and S. D. Levene, *Q. Rev. Biophys.* **25**, 171 (1992).
5. L. S. Lerman and H. L. Frisch, *Biopolymers* **21**, 995 (1982).
6. O. J. Lumpkin and B. H. Zimm, *ibid.*, p. 2315.
7. O. J. Lumpkin, P. Dejardin, B. H. Zimm, *ibid.* **24**, 1573 (1985).
8. G. W. Slater and J. Noolandi, *Phys. Rev. Lett.* **55**, 1579 (1985); *Biopolymers* **25**, 431 (1986).
9. J. Noolandi, J. Rousseau, G. W. Slater, *Phys. Rev. Lett.* **58**, 2428 (1987).
10. J. M. Deutsch, *ibid.* **59**, 1255 (1987); *Science* **240**, 922 (1988).
11. J. L. Viovy, *Phys. Rev. Lett.* **60**, 855 (1988).
12. J. Noolandi, G. W. Slater, H. A. Lim, J. L. Viovy, *Science* **243**, 1456 (1989).
13. P. Dejardin, *Phys. Rev. A* **40**, 4752 (1989).
14. B. H. Zimm, *Phys. Rev. Lett.* **61**, 2965 (1988); *J. Chem. Phys.* **94**, 2187 (1991).
15. J. M. Deutsch, *J. Chem. Phys.* **90**, 7436 (1989).
16. H. A. Lim, G. W. Slater, J. Noolandi, *ibid.* **92**, 709 (1990).
17. J. M. Schurr and S. B. Smith, *Biopolymers* **29**, 1161 (1990).
18. M. O. de la Cruz, J. M. Deutsch, S. F. Edwards, *Phys. Rev. A* **33**, 2047 (1986); these authors explicitly assume frictionless contact between the polymer and the gel.
19. M. O. de la Cruz, D. Gersappe, E. O. Shaffer, *Phys. Rev. Lett.* **64**, 2324 (1990).
20. E. O. Shaffer and M. O. de la Cruz, *Macromolecules* **22**, 1351 (1989).
21. T. A. J. Duke, *Phys. Rev. Lett.* **62**, 2877 (1989); *J. Chem. Phys.* **93**, 9055 (1990).
22. T. L. Madden and J. M. Deutsch, *J. Chem. Phys.* **94**, 1584 (1991).
23. J. M. Deutsch and J. D. Reger, *ibid.* **95**, 2065 (1991).
24. T. A. J. Duke and J. L. Viovy, *Phys. Rev. Lett.* **68**, 542 (1992); *J. Chem. Phys.* **96**, 8552 (1992).
25. G. W. Slater, *J. Phys. II* **2**, 1149 (1992).
26. N. H. Frank, *Introduction to Mechanics and Heat* (McGraw-Hill, New York, 1939), p. 55.
27. S. B. Smith and A. J. Bendich, *Biopolymers* **29**, 1167 (1990).
28. S. B. Smith, P. K. Aldridge, J. B. Callis, *Science* **243**, 203 (1989).
29. Intersegment forces can be included. For example, for elastic forces, the tension in Eq. 4 would be replaced by:

    $$T(r) = -\gamma \frac{dr(n)}{dn}$$

    where γ is the elastic force constant, and $\rho = dn/dr$ and ε are no longer constant.
30. The general result for the steady-state velocity of an entangled chain through a coarse-grained tube of length L with tension $T(0)$ at one end and $T(L)$ at the other end is

    $$\frac{\beta v}{\alpha\mu} = \frac{\exp(-\alpha\mu\rho L)T(0) - T(L)}{1 - \exp(-\alpha\mu\rho L)} + \frac{qE\int_0^L \exp(\alpha\mu\rho x)\cos[\theta(x)]dx}{\exp(\alpha\mu\rho L) - 1}$$

    Trapping of the entangled chain occurs from regions where $\cos[q(x)]$ is negative.
31. When the segment velocity approaches zero, it is necessary to take into account the influence of thermal fluctuation, which is not included in our analysis. These thermal fluctuations lead to polymer motion, therefore modifying the results quoted here as $v \rightarrow 0$.
32. The coarse graining excludes end effects, which lead to small corrections that do not depend on polymer length.
33. S. D. Levene and B. H. Zimm, *Proc. Natl. Acad. Sci. U.S.A.* **84**, 4054 (1987).
34. C. R. Calladin, C. M. Collis, H. R. Drew, M. R. Mott, *J. Mol. Biol.* **221**, 981 (1991); see also E. Avranitdou and D. Hoagland, *Phys. Rev. Lett.* **67**, 1461 (1991) and D. L. Smisek and D. A. Hoagland, *Science* **248**, 1221 (1990).
35. In some off-lattice simulations (*18–22*), the rules for chain movement include rejection of the move (in contrast to elastic reflection) if the chain encounters a gel point. This approach implicitly corresponds to an inelastic collision, which is required for solid friction.
36. The temperature dependence of the mobility could be quite different if solid friction is present in addition to viscous friction from the solvent.
37. J.D. thanks G. M. Whitesides for helpful discussions.

29 January 1993; accepted 16 April 1993

A Bimetallic Hydroformylation Catalyst: High Regioselectivity and Reactivity Through Homobimetallic Cooperativity

Melanie E. Broussard, Booker Juma, Spencer G. Train,
Wei-Jun Peng, Scott A. Laneman, George G. Stanley*

The *racemic* and *meso* diastereomers of an electron-rich binucleating tetraphosphine ligand have been used to prepare homobimetallic rhodium norbornadiene complexes. The *racemic* bimetallic Rh complex is an excellent hydroformylation catalyst for 1-alkenes, giving both a high rate of reaction and high regioselectivity for linear aldehydes, whereas the *meso* complex is considerably slower and less selective. A mechanism involving bimetallic cooperativity between the two rhodium centers in the form of an intramolecular hydride transfer is proposed. Mono- and bimetallic model complexes in which the possibility for bimetallic cooperativity has been reduced or eliminated are very poor catalysts.

Hydroformylation (also called "oxo"), the world's largest industrial homogeneous catalytic process, produces more than 5 billion kilograms of aldehydes and alcohols each year (*1*). In this process, alkenes react with hydrogen and carbon monoxide to give either linear or branched aldehydes (Eq. 1; R, alkyl).

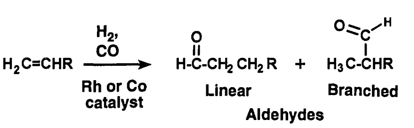

$$H_2C{=}CHR \xrightarrow[\text{Rh or Co catalyst}]{H_2,\ CO} H\text{-}\overset{O}{\overset{\|}{C}}\text{-}CH_2CH_2R + H_3C\text{-}\overset{O=C\text{-}H}{\overset{|}{C}}HR \qquad (1)$$

Monometallic rhodium triphenylphosphine (Rh/PPh_3) catalysts dominate the industry, particularly for C_3 through C_6 1-alkenes, where regioselectivity in making the more valuable linear aldehyde products is critical.

Demonstrating that two or more metal centers can cooperate in a homogeneous catalytic process to produce a better catalyst compared to monometallic systems has been a major goal of our research. Several groups have reported dimer and cluster catalysis of hydroformylation (*2*). None of these polymetallic catalysts, however, combine high product regioselectivities with high reaction rates, and none of them compare favorably to commercial Rh/PPh_3 monometallic catalysts. We have designed a tetraphosphine ligand that can simultaneously bridge and chelate two metal centers to create bimetallic complexes with considerable conformational flexibility. This ligand, $(Et_2PCH_2CH_2)(Ph)PCH_2P(Ph)(CH_2CH_2PEt_2)$ (et,ph-P4; Et, ethyl), has *racemic* (**1r**) and *meso* (**1m**) diastereomers (*3*). We have characterized bimetallic complexes of **1r** and **1m** in which the two metals are separated or bonded to one another (*4*).

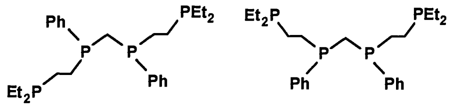

***racemic* - et,ph-P4**
1r

***meso* - et,ph-P4**
1m

The reaction of **1r** or **1m** (*5*) with two equivalents of $[Rh(nbd)_2](BF_4)$ (nbd = norbornadiene) produces the bimetallic complexes $[Rh_2(nbd)_2(\text{et,ph-P4})](BF_4)_2$ (*racemic* **2r**, and *meso* **2m**) in high yield (*6*). An x-ray crystal structure determination (*7*) of **2r** (Fig. 1) shows that the et,ph-P4 ligand bridges and chelates the two square-planar Rh centers, as observed in previous bimetallic complexes of et,ph-P4. There is no Rh–Rh bonding in this complex, and the metals are separated by 5.505 Å. The ^1H and ^{31}P nuclear magnetic resonance (NMR) spectra for **2m** point to a bridged and chelated bimetallic structure similar to

---

Department of Chemistry, Louisiana State University, Baton Rouge, LA 70803–1804.

*To whom correspondence should be addressed.

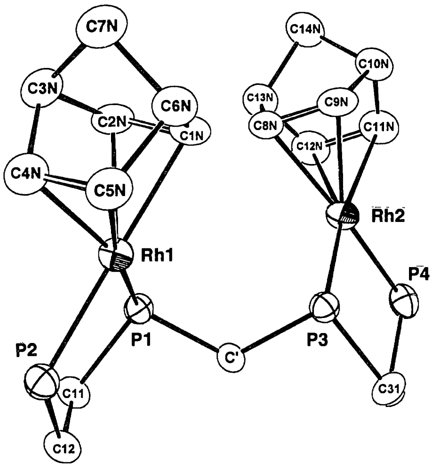

Fig. 1. An ORTEP plot of x-ray structure of *racemic*-$Rh_2(nbd)_2(et,ph\text{-}P4)^{2+}$, **2r**. The ethyl and phenyl groups on the et,ph-P4 ligand, and all hydrogen atoms, are omitted for clarity. Some key bond distances and angles are: Rh1 ··· Rh2 = 5.5058(6) Å; Rh1–P1 = 2.319(2) Å; Rh1–P2 = 2.281(2) Å; Rh1–C1N = 2.249(6) Å; Rh1–C2N = 2.237(6) Å; Rh1–C4N = 2.198(6) Å; Rh1–C5N = 2.217(6) Å; P1–Rh1–P2 = 83.84(6)°; P1–Rh1–C1N = 109.4(2)°; P1–Rh1–C2N = 101.6(2)°; P1–Rh1–C4N = 149.5(2)°; P1–Rh1–C5N = 172.5(2)°; C2N–Rh1–C5N = 77.7(2)°; C1N–Rh1–C4N = 77.4(2)°; and P1–C′–P3 = 120.2(3)°. Numbers in parentheses are errors in the last digit.

that seen for *meso*-Ni_2Cl_2(et,ph-P4) (*8*).

Compound **2r** is a precursor to an active, highly regioselective bimetallic catalyst proposed as *racemic*-$Rh_2H_2(CO)_2$(et,ph-P4) (**3r**) for the hydroformylation of 1-alkenes (*9*). We have used 1-hexene as our standard (Table 1), but the results presented are typical for 1-alkenes (*10*). In comparing **2r** to the commercial Rh/PPh_3 catalyst (Table 1), we find that **2r** is ~40% faster and has a higher linear-to-branched aldehyde regioselectivity (*11*), whereas the *meso* catalyst precursor **2m** generates the poorer hydroformylation catalyst *meso*-$Rh_2H_2(CO)_2$(et,ph-P4) (**3m**). The *racemic* catalyst is 12 times faster than the *meso* catalyst and gives considerably higher overall product selectivities (Table 1), particularly with respect to the undesirable alkene isomerization side reactions, which build up significantly over longer periods of time for **3m**. Reasons for the rate and regioselectivity differences between **3r** and **3m** are discussed below.

In contrast with virtually all other aryl phosphine– or phosphite-coordinated Rh hydroformylation catalysts, **3r** does not require any excess phosphine ligand (PPh_3) in order to maintain its selectivity or stability (*12*). The need for excess PPh_3 in monometallic Rh catalysts arises from the relatively weak Rh–PPh_3 (or phosphite) bonding. In order to maintain the coordination of two PPh_3 ligands, which are required for good regioselectivity, a large excess of PPh_3 is required to force the dissociation equilibrium to favor $HRh(CO)(PPh_3)_2$ (*13*). In **3r**, the chelating and electron-donating et,ph-P4 phosphine ligand coordinates strongly enough to the Rh centers so that excess phosphine is not needed.

The absence of a Rh–Rh bond in **2r** and **3r** allows us to readily prepare monometallic model complexes that represent "half" of the catalyst. This simple first test explores whether each Rh center is functioning as a conventional monometallic catalyst. $[Rh(nbd)(P_2)](BF_4)$ catalyst precursors were prepared with the following four bisphosphine ligands with different electron-donating substituents: $Et_2PCH_2CH_2PEt_2$ (depe), which is electron rich relative to et,ph-P4; $Et_2PCH_2CH_2P(Me)Ph$ (depmpe), the closest electronic analog to one-half of et,ph-P4; $Et_2PCH_2CH_2PPh_2$ (dedppe), which is slightly less electron rich; and $Ph_2PCH_2CH_2PPh_2$ (dppe), which is moderately less electron rich.

All four monometallic complexes are extremely poor hydroformylation catalysts. They show less than 2% conversion of alkene to aldehyde product after 3 hours, low linear-to-branched selectivities of 3:1 or less, and considerable amounts of undesirable alkene isomerization and hydrogenation (Table 1). The activity and regioselectivity of **3r** is, therefore, opposite that of monometallic Rh complexes with electron-rich ethylene-bridged chelating phosphines. This result agrees with the limited previous work on electron-rich phosphine ligands (*14*) and indicates that **3r** uses some sort of bimetallic cooperativity to effect high regioselectivities and high reaction rates.

Any discussion of bimetallic mechanisms should take into account the early work on cobalt-catalyzed hydroformylation (*15*). A monometallic mechanism was proposed that has become the generally accepted pathway (*16*) for both Co and Rh catalysts. A more speculative bimetallic mechanism was also suggested involving an intermolecular hydride transfer from $HCo(CO)_4$ to $Co(acyl)(CO)_4$. Elimination of the aldehyde product then produces $Co_2(CO)_8$, which reacts with H_2 to break the Co–Co bond to reform two $HCo(CO)_4$ molecules. This suggests an interesting mechanistic possibility for our catalyst.

In **3r**, the conformational flexibility of the et,ph-P4 ligand and the constrained proximity of the two metal centers should dramatically increase the probability of an intramolecular hydride transfer. We propose just such a mechanism for **3r** (Fig. 2) in which bimetallic cooperativity, via an intramolecular hydride transfer, facilitates the elimination of aldehyde from the acyl intermediate. This mechanism, which we offer as a hypothesis to be tested, uses proximity for catalytic power just as many bioorganic models of enzyme catalysts do (*17*).

Table 1. Results from the hydroformylation of 1-hexene in acetone at 90°C and 90 psig H_2-CO after 3 hours. Numbers in parentheses are the errors in the last digit or digits.

Catalyst	k^*_{obs} (min^{-1})	Initial turnover rate (min^{-1})	Alkene conversion to aldehyde (%)	Linear-to-branched aldehyde ratio†	Alkene isomerization (%)	Alkene hydrogenation (%)
racemic-$Rh_2(nbd)_2(et,ph\text{-}P4)^{2+}$, **2r**	0.0238 (8)	10.6 (5)	85 (1)	27.5 (8)	8 (1)‡	3.4 (3)‡
$Rh(acac)(CO)_2$ with 0.82 M PPh_3	0.016 (2)	9 (1)	86 (3)	17 (2)	2.5 (4)	2.8 (3)
meso-$Rh_2(nbd)_2(et,ph\text{-}P4)^{2+}$, **2m**		0.9 (1)	16 (3)	14 (2)	4.1 (7)	2.3 (3)
$Rh(nbd)(depe)^+$		0.017 (2)	0.9 (2)	2 (2)	16 (1)	5.2 (9)
$Rh(nbd)(depmpe)^+$		0.025 (3)	1.7 (6)	3 (1)	50 (1)	15.3 (4)
$Rh(nbd)(dedppe)^+$		0.020 (3)	1.1 (1)	3.1 (2)	42 (3)	14.0 (4)
$Rh(nbd)(dppe)^+$		0.040 (6)	1.2 (3)	2.6 (6)	51 (3)	14 (3)
$Rh_2(nbd)_2(et,ph\text{-}P4\text{-}propyl)^{2+}$, **9(r + m)**		0.097 (3)	1.7 (1)	2.4 (1)	59 (2)	16 (1)
$Rh_2(nbd)_2$(et,ph-P4-*p*-xylyl)$^{2+}$, **10(r + m)**		0	0		60.1 (8)	17 (1)
$Rh_2(nbd)_2(et,ph\text{-}P4)^{2+}$, **2(r + m)**	0.0102 (11)	4.1 (1)	80 (1)	20.5 (6)	9.8 (2)	4.5 (1)

*Pseudo first-order rate constant based on gas uptake; 1 mM catalyst concentration; average of at least four runs. Rate constants not listed could not be accurately calculated because of the slowness of the reactions and associated side reactions. †The regioselectivity was constant throughout the course of a run. ‡The relatively high amounts of alkene isomerization and hydrogenation are side reactions caused by the production of HBF_4 generated when **2r** reacts with H_2 to form **3r**. Addition of two equivalents of a neutral base, such as NEt_3, causes both the isomerization and hydrogenation to fall to less than 1.5% and increases the product regioselectivity to greater than 30:1. Unfortunately, the amine bases used so far slow the catalyst somewhat due to what we believe is competitive binding to the Rh centers.

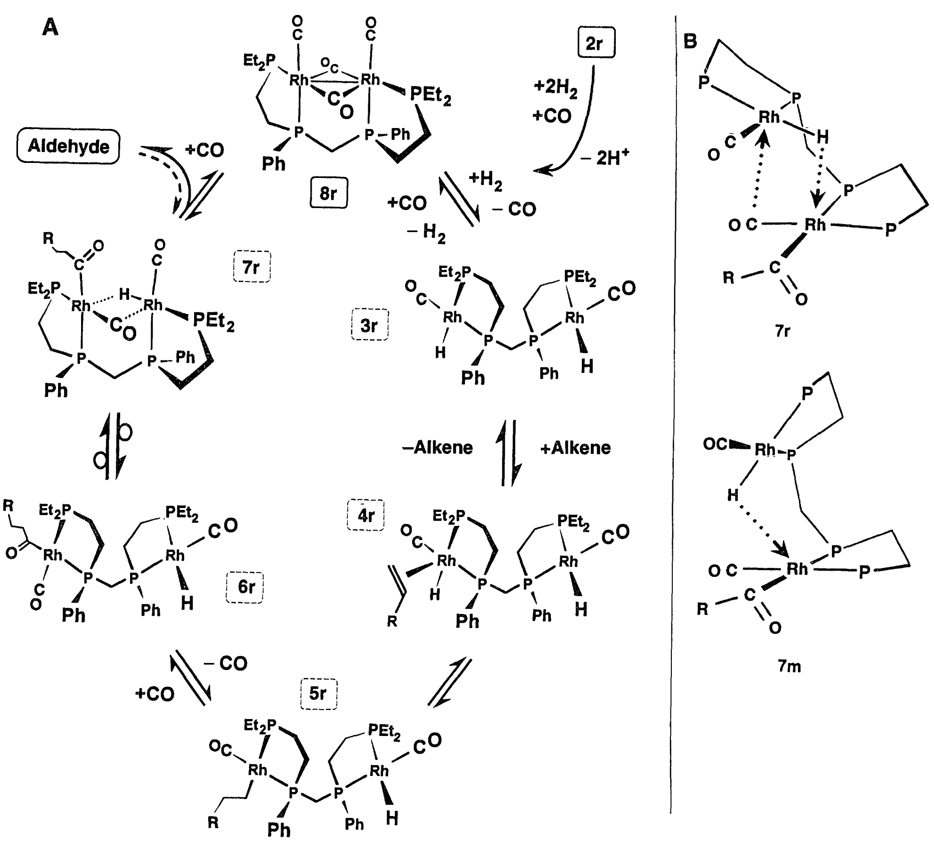

Fig. 2. (**A**) Proposed mechanism for bimetallic hydroformylation. (**B**) Schematic representations of the closed-mode structures for the proposed hydride transfer step in the *racemic*- and *meso*-Rh(acyl)(CO)(et,ph-P4)RhH(CO) intermediates (or transition states), **7r** and **7m**. Both molecules have similar energies from full molecular dynamics minimizations, although the modeling cannot calculate the electronic orbital effects caused by interaction of the bridging ligands with the Rh centers. **7r** can form a double-bridging interaction with the hydride of the top Rh interacting with the bottom acyl-bound Rh, while the carbonyl group on the bottom Rh is able to donate electron density via its π system to the upper Rh atom. **7m** can form only a single bridging interaction, which we believe contributes to a higher energy reaction pathway.

The first several steps in the proposed mechanism are essentially the same as those established for monometallic Rh/PPh_3 catalysts: (i) addition of H_2 and CO to **2r** produces **3r**, the proposed active catalyst; (ii) coordination of alkene to **3r** makes **4r**; (iii) alkene insertion into the Rh–H bond gives the linear (or branched) alkyl species **5r**; and (iv) coordination of CO, followed by CO insertion into the Rh-alkyl group yields the acyl complex **6r**. In monometallic systems, the next step is addition of H_2 to produce a Rh(III) dihydride species that can then eliminate aldehyde product. This step, generally believed to be the rate-determining step (*18*), is particularly slow with electron-rich phosphine ligands because Rh(I) prefers to bind another CO over H_2 (*19*). Compound **3r** avoids this potential problem by having a proximate Rh-H moiety, which intramolecularly transfers a hydride to facilitate the aldehyde elimination (**7r** → **8r**).

Although the extremely poor activities and selectivities of the monometallic models provide one piece of evidence supporting bimetallic cooperativity, this idea needed further support. We reasoned that if the two metal centers cannot get near one another then they will not be able to cooperate and catalysis will stop. Two new tetraphosphine ligands have been prepared in which the central methylene bridge is replaced by larger spacers—one, a rigid *p*-xylylene spacer (et,ph-P4-*p*-xylylene), and the other, a more flexible 1,3-propylene spacer (et,ph-P4-propyl).

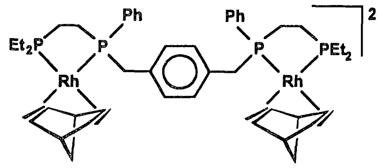

9(r+m)

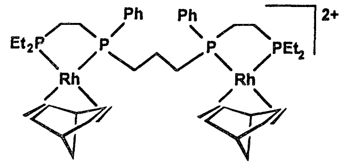

10(r+m)

These spaced-tetraphosphine ligands have essentially the same electronic donor properties as et,ph-P4, but keep the two metals apart. Mixed *racemic* and *meso* bimetallic Rh/nbd complexes (1:1 mixtures from NMR measurements) have been prepared from each spaced tetraphosphine ligand [**9(r + m)** and **10(r + m)**]. Both sets of spaced bimetallic complexes are very poor hydroformylation catalysts with 1-hexene (*20, 21*). The very low rates and regioselectivities are analogous to the model monometallic results (Table 1).

Additional evidence supporting the bimetallic mechanism comes from SYBYL (*22*) molecular modeling studies (*23*), which help explain the difference in activity between **3r** and **3m**. The bimetallic acyl intermediate, *racemic*-Rh(acyl)(CO)(et,ph-P4)RhH(CO), **6r**, can readily rotate about the central CH_2 bridge to form a doubly bridged intermediate species, **7r**. The hydride bridges to the acyl-bound Rh, while the CO ligand on the acyl Rh can bridge to the hydrido-bound Rh (Fig. 3). The *meso* analog, **7m**, however, can only form a single bridge via the hydride to the acyl-bound Rh center (Fig. 2B). The CO ligand in **7m** is not oriented properly to bridge to the upper Rh. We believe that the second bridging interaction, present in the *racemic* complex, favors the intramolecular hydride transfer by stabilizing the Rh–H bond-breaking step. The donation of π electron density from the bridging CO in **7r** will lower the energy of the formally three-coordinate, high-energy Rh center that remains after the hydride ligand is transferred to the acyl-bound Rh.

The second bridging interaction in **7r** may play an even more important role in the subsequent reductive elimination step that generates a relatively high-energy Rh(−1) oxidation state on the one metal center. The close proximity of the second Rh atom in a +1 oxidation state will favor electron transfer to give two Rh(0) centers with an energy-lowering Rh–Rh bond to produce **8r**. Oxidative addition of H_2 to this electron-rich, reactive dimer cleaves the Rh–Rh bond to regenerate the starting catalyst **3r**. Isolation of **8r**, from reaction of **2r** with H_2 and CO (*24*), suggests a fairly facile H_2 addition-loss equilibrium between **8r** and **3r**, consistent with previous work on related Rh complexes (*25*). Although the *meso* bimetallic catalyst **3m** can also utilize bimetallic cooperativity, we believe that it has to proceed through a higher energy pathway because of the stereochemical differences between the *meso* and *racemic* et,ph-P4 ligands. This results in slower catalytic rates relative to the *racemic* catalyst, but better than the monometallic or spaced-bimetallic model complexes.

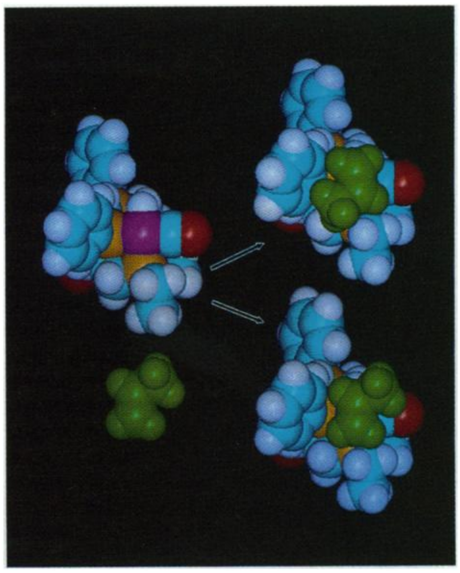

Fig. 3. Space-filling models of the *racemic*-$Rh_2H_2(CO)_2$(et,ph-P4) catalyst, **3r**, with a propylene molecule docked to one face. Except for the propylene, which is colored green, the coloring scheme for the atoms is as follows: Rh (magenta); P (orange); O (red); C (cyan); and H (white). In all three views, the catalyst is oriented the same with the Rh–H bond pointing up. The top right-hand view has the propylene docked in the proper orientation for the branched product (pro-branched complex), whereas the bottom view has the propylene oriented for the linear product (pro-linear complex). The Rh in both propylene-bound views is completely covered by the propylene molecule. Note that the alkene orbitals line up well with the Rh–H bond to allow a hydride transfer to the terminal carbon of the double bond in the top system, and to the internal carbon of the double bond in the bottom view. This geometry leads to the branched and linear alkyl intermediates, respectively. The pro-branched complex in the top view is calculated to be 7.5 kcal/mol higher in energy than the pro-linear species. The unfavorable steric interactions in the pro-branched complex can be clearly seen between the propylene's methyl group and the phenyl and ethyl groups on the P atoms.

The bimetallic cooperativity in the proposed mechanism represents a very effective way of performing hydroformylation. The fundamental concept of a hydride transfer between two metal centers has been studied and shown to occur in stoichiometric model reactions by numerous groups (*26*). $Rh_2(\mu\text{-S-}t\text{-Bu})_2(CO)_2(PPh_3)_2$ is another hydroformylation catalyst for which bimetallic cooperativity has been proposed (*27*). However, the reaction rates and regioselectivities of $Rh_2(\mu\text{-S-}t\text{-Bu})_2(CO)_2(PPh_3)_2$ very closely resemble those of Rh/PR_3 monometallic catalysts, indicating that the active catalyst may be monometallic in nature (*28*), quite unlike **3r**.

We believe that the high linear aldehyde regioselectivity arises from the shape of **3r**. When an alkene coordinates to **3r** (Fig. 3), it will likely add to the exo coordination site of either Rh center. As it coordinates to the Rh, the other ligands will bend away to form a trigonal bipyramid (or square pyramid), which is the least congested coordination geometry. Compound **3r**, however, cannot attain this ideal geometry because the other half of the face-to-face bimetallic complex limits the motion of the ligand environment away from the coordinating alkene toward trigonal bipyramidal (or square pyramidal). Minimizing the geometric reorganization about the Rh maximizes the et,ph-P4 ligand's steric effect, directing the alkene insertion into the M–H bond to form a linear alkyl group, which goes on to form the linear aldehyde.

Molecular dynamics minimizations of a propylene molecule docked to **3r** suggest a 7.5-kcal/mol preference for the coordination of alkene to the Rh center to give the linear alkyl product (Fig. 3). This result is qualitative as molecular modeling only gives information on steric factors in the **3r**-propylene complex. Regioselectivity arises from energy differences in transition states, where many steric and electronic effects operate. Attributing the origin of the aldehyde regioselectivity to the initial alkene coordination and hydride insertion step is consistent with the best evidence from monometallic Rh/PPh_3 catalysts (*29*). This step is not believed to be reversible in a good hydroformylation catalyst.

One unusual feature of **3r** is that high concentrations of 1-hexene inhibit hydroformylation catalysis, an effect not observed for monometallic hydroformylation catalysts, but one consistent with the proposed bimetallic mechanism. Addition of two alkene molecules to **3r** would ultimately lead to a bimetallic species that has one acyl group on each metal and no hydride ligand, which is needed for the intramolecular transfer and subsequent aldehyde product elimination.

REFERENCES AND NOTES

1. B. Cornils, in *New Syntheses with Carbon Monoxide*, J. Fable, Ed. (Springer-Verlag, Berlin, 1980); C. A. Tolman and J. W. Faller, in *Homogeneous Catalysis with Metal Phosphine Complexes*, L. H. Pignolet, Ed. (Plenum, London, 1983).
2. R. C. Ryan, C. U. Pittman, Jr., P. C. O'Connor, *J. Am. Chem. Soc.* **99**, 1986 (1977); A. Ceriotti, L. Garlaschelli, G. Longoni, M. C. Malatesta, D. Strumolo, *J. Mol. Catal.* **24**, 323 (1984); M. Hidai, A. Fukuoka, Y. Koyasu, Y. Uchida, *ibid.* **35**, 29 (1986); P. Kalck, J.-M. Frances, P-M. Pfister, T. G. Southern, A. Thorez, *J. Chem. Soc. Chem. Commun.* **1983**, 510 (1983); P. Kalck, *Pure Appl. Chem.* **61**, 967 (1989); M. G. Richmond, M. Absi-Halbi, C. U. Pittman, Jr., *J. Mol. Catal.* **22**, 367 (1984); A. R. Sanger, *ibid.* **3**, 221 (1977–78); A. R. Sanger, *J. Chem. Soc. Dalton Trans.* **1977**, 1971 (1977); G. Süss-Fink and G. Herrmann, *J. Chem. Soc. Chem. Commun.* **1985**, 735 (1985).
3. S. A. Laneman, F. R. Fronczek, G. G. Stanley, *J. Am. Chem. Soc.* **110**, 5585 (1988).
4. ———, *Inorg. Chem.* **28**, 1206 (1989).
5. G. G. Stanley *et al.*, unpublished results.
6. Synthesis of $[Rh_2(nbd)_2(\text{et,ph-P4})](BF_4)_2$: The *racemic*- or *meso*-et,ph-P4 ligand (2.32 g, 5.0 mmol) in 5 ml of CH_2Cl_2 was added dropwise to a CH_2Cl_2 (15-ml) solution of $[Rh(nbd)_2]BF_4$ (3.74 g, 10.0 mmol) with stirring. The resulting solution was added slowly to 150 ml of rapidly stirred ether to obtain an orange precipitate of the bimetallic metal complex (yield: 5.0 g, 98%). **2m**: $^{31}P\{^1H\}$ NMR (40.25 MHz, CD_2Cl_2, versus 85% H_3PO_4): δ 58.7 (dd, coupling constant J_{P-Rh} = 150 Hz and J_{P-P} = 23 Hz), 46.9 (doublet of multiplets, J_{P-Rh} = 156 Hz). **2r**: $^{31}P\{^1H\}$ NMR (40.25 MHz, CD_2Cl_2, versus 85% H_3PO_4): δ 58 (dd, J_{P-Rh} = 150 Hz and J_{P-P} = 23 Hz), 47.5 (doublet of multiplets, J_{P-Rh} = 156 Hz).
7. X-ray data: triclinic, $P\bar{1}$, a = 14.695(2) Å, b = 16.574(2) Å, c = 11.980(2) Å, α = 109.32(2)°, β = 106.63(2)°, γ = 97.91(2)°, V = 2549(3) Å^3 (numbers in parentheses are the errors in the last digits), MoKα radiation, Z = 2, absorption coefficient = 16.4 cm^{-1} (empirical absorption correction done using psig scans), 4508 observed data [$I > 3\sigma(I)$], 559 variables refined, R = 0.0531, R_w = 0.0581, goodness of fit = 2.87. Coordinates will be deposited with the Cambridge Crystallographic Database.
8. S. A. Laneman, F. R. Fronczek, G. G. Stanley, *Inorg. Chem.* **28**, 1872 (1989).
9. Experimental data for catalytic runs: **2r** (0.090 g, 0.0875 mmol) was dissolved in 80 ml of acetone under inert atmosphere conditions in a Schlenk flask. The solution was transferred to a 150-ml capacity Parr autoclave under an inert atmosphere. 1-Hexene (10 ml, 6.73 g, 80 mmol) was added under inert atmosphere conditions to an external addition cylinder connected to the autoclave. The autoclave was heated to 90°C and stirred at 1000 rpm with approximately one-half the desired operating pressure (~45 psi) of a 1:1 H_2-CO gas mixture. When the autoclave stabilized at 90°C (~65 psi), the olefin addition cylinder was pressurized with H_2-CO and the olefin was transferred into the autoclave. An initial sample was taken, and data collection was begun. All runs were done at constant pressure. Samples from the autoclaves (1 to 2 ml) were taken hourly and analyzed by gas chromatography (and occasionally NMR) for product distributions.
10. The catalyst has been studied with propylene, 1-hexene, and 1-octene, all with similar results. The catalyst has been independently tested by Union Carbide Corp. (J. Babin) and Hoechst-Celanese Corp. (J. Unruh). Independent results from Hoechst-Celanese on the hydroformylation of 1-hexene with the *racemic* and *meso* catalysts agree with the values reported here.
11. The rate and selectivity of Rh/PPh_3 hydroformylation catalysts are quite dependent on the concentration of PPh_3. We used higher PPh_3 concentration conditions that favor higher linear-to-branched aldehyde regioselectivities but slower reaction rates.
12. We have achieved >12,000 turnovers in a single batch run for the hydroformylation of 1-hexene with no signs of catalyst decomposition.
13. R. L. Pruett and J. A. Smith, *J. Org. Chem.* **34**, 327 (1969); R. V. Kastrup, J. S. Merola, A. A. Oswald, **196**, 43 (1982); J. M. Brown and A. G. Kent, *J. Chem. Soc. Perkin Trans.* **1987**, 1597 (1987).
14. J. D. Unruh and J. R. Christenson, *J. Mol. Catal.* **14**, 19 (1982); G. Consiglio and F. Rama, *ibid.* **66**, 1 (1991).
15. D. S. Breslow and R. F. Heck, *Chem. Ind. (London)* **1960**, 467 (1960); R. F. Heck and D. S. Breslow, *J. Am. Chem. Soc.* **83**, 4024 (1961).
16. M. F. Mirbach, *J. Organomet. Chem.* **265**, 205 (1984); W. R. Moser, *Adv. Chem. Ser.* **230**, 3 (1992).
17. H. A. Saroff, *Biochemistry* **30**, 10085 (1991); R. D. Gandour, in *Transition States of Biochemical Pro-*

cesses, R. D. Gandour and R. L. Schowen, Eds. (Plenum, New York, 1978), pp. 529–552.

18. R. L. Pruett, *Adv. Organomet. Chem.* **17**, 1 (1979); D. Evans, J. A. Osborn, G. Wilkinson, *J. Chem. Soc. A* **1968**, 3133 (1968).
19. W. R. Moser, C. J. Papile, D. A. Brannon, R. A. Duwell, S. J. Weininger, *J. Mol. Catal.* **41**, 271 (1987); C. Bianchini, A. Meli, M. Peruzzini, F. Vizza, *Organometallics* **9**, 226 (1990).
20. S. A. Laneman and G. G. Stanley, *Adv. Chem. Ser.* **230**, 349 (1992); note that all experimental rates presented in this reference are twice their correct values.
21. We did not test the individual *racemic* and *meso* complexes for the spaced catalysts because of the poor catalysis. Hydroformylation runs with a 1:1 mixture of **2r** and **2m** showed an average of their individual rates and regioselectivies (Table 1); we presume that any good catalysis by either diastereomer of **9** or **10** would have been observable in the mixed catalyst.
22. TRIPOS Associates, Inc., 1699 South Hanley Road, Suite 303, St. Louis, MO 63144.
23. A simple average force field was used about the metal center having a relatively strong bond-stretching component, but only a medium to weak bond-angle bending term. (G. Stanley, paper presented at the SYBYL Users Meeting, May 1992, St. Louis, MO).
24. Spectroscopic data for *racemic*-$Rh_2(\mu\text{-}CO)_2(CO)_2$(et,ph-P4): dark red oil; infrared spectra ν_{CO}: 1985 cm^{-1} (sh), 1957 cm^{-1} (s), 1813 cm^{-1} (sh), 1768 cm^{-1} (m); $^{31}P\{^1H\}$ NMR (40.48 MHz, acetone-d_6, versus 85% H_3PO_4): δ 71.6 (dt, 1P, $J_{P\text{-}Rh}$ = 96 Hz and $J_{P\text{-}P}$ = 23 Hz), 26.0 (dt, 1P, $J_{P\text{-}Rh}$ = 96 Hz and $J_{P\text{-}P}$ = 23 Hz).
25. B. R. James, D. Mahajan, S. J. Rettig, G. M. Williams, *Organometallics* **2**, 1452 (1983); C. Allevi, M. Golding, B. T. Heaton, C. A. Ghilardi, S. Midollini, A. Orlandini, *J. Organomet. Chem.* **326**, C19 (1987); P. Singh, C. B. Dammann, D. J. Hodgson, *Inorg. Chem.* **12**, 1335 (1973); D. Evans, G. Yagupsky, G. Wilkinson, *J. Chem. Soc. A* **1968**, 2660 (1968).
26. W. D. Jones, J. M. Huggins, R. G. Bergman, *J. Am. Chem. Soc.* **103**, 4415 (1981); M. J. Nappa, R. Santi, J. Halpern, *Organometallics* **4**, 34 (1985); B. D. Martin, K. E. Warner, J. R. Norton, *J. Am. Chem. Soc.* **108**, 33 (1986); K. E. Warner and J. R. Norton, *Organometallics* **4**, 2150 (1985); F. Ungváry and L. Markó, *ibid.* **2**, 1608 (1983).
27. P. Kalck, *Polyhedron* **7**, 2441 (1988).
28. R. Davis, J. W. Epton, T. G. Southern, *J. Mol. Catal.* **77**, 159 (1992).
29. R. Lazzaroni, G. Uccello-Barretta, M. Benetti, *Organometallics* **8**, 2323 (1989).

30. Supported by the National Science Foundation grants CHE-88-23041 and CHE-92-01051, the Louisiana Educational Quality Support Fund grant LEQSF(1990–93)-RD-B-07, Hoechst-Celanese Corporation, ARCO Chemical Company, Exxon Educational Foundation, and the LSU Center for Energy Studies. We thank F. R. Fronczek for providing the x-ray crystal structure analysis on **2r**, and R. D. Gandour and A. W. Maverick for very helpful comments on the manuscript.

2 February 1993; accepted 21 April 1993

Paleoatmospheric Signatures in Neogene Fossil Leaves

Johan Van Der Burgh, Henk Visscher,* David L. Dilcher, Wolfram M. Kürschner

An increase in the atmospheric carbon dioxide (CO_2) concentration results in a decrease in the number of leaf stomata. This relation is known both from historical observations of vegetation over the past 200 years and from experimental manipulations of microenvironments. Evidence from stomatal frequencies of fossil *Quercus petraea* leaves indicates that this relation can be applied as a bioindicator for changes in paleoatmospheric CO_2 concentrations during the last 10 million years. The data suggest that late Neogene CO_2 concentrations fluctuated between about 280 and 370 parts per million by volume.

Analysis of air locked in polar ice has been used to document the paleoatmospheric CO_2 concentration for the past 160,000 years (*1*). Concentrations of CO_2 from before this time cannot be directly measured and can only be inferred from forward modeling of the CO_2 global budget (*2*) or from proxy records that are based on geochemical or paleontological observations. The geochemical approach depends on the interpretation of changing $^{13}C/^{12}C$ isotope ratios in the marine carbonate record (*3*) and, more recently, on the analysis of $^{13}C/^{12}C$ ratios of soil carbonates (*4*). A relevant paleontological approach is highly dependent on the ecophysiological interpretation of the morphological or anatomical characteristics of fossils (*5*). Because of the prominent role of photosynthetic CO_2 fixation in the interaction between the atmosphere and biota through time, land plants represent one of the most obvious categories of organisms to be investigated for paleoatmospheric signatures. In this report, we illustrate that the analysis of stomatal frequencies on fossil leaves may be used to determine CO_2 concentrations during the last 10 million years.

Physical models of CO_2 fixation in land plants with C_3 metabolism (*6*) can be used to show that the areal density of leaf stomata is responsive to changes in ambient CO_2 concentration. Under nonlimiting light and water conditions, leaves have an optimal CO_2 fixation rate at a stomatal conductance to diffusion of CO_2 at which the CO_2 concentration is maintained in the leaf interior at the break point between saturation and limitation of the CO_2 receptor molecule ribulose biphosphate (RuP_2). The stomatal conductance to diffusion is a complex parameter that is dominated by the density and the aperture size of the stomata. The maintenance of optimal CO_2 fixation may require that an increase of atmospheric CO_2 concentration be accompanied by a lower value of the stomatal conductance. Hence, if we assume that differences in stomatal frequency are part of the phenotypic plasticity of a plant species, such a lowering could be reached through a decline of stomatal density (*7*).

This possibility is supported by the results from the study of herbarium material collected over the last 200 years. Research by Woodward (*8*) emphasized that the human-induced CO_2 increase has resulted in a mean reduction of 40% in the stomatal density of European temperate forest trees. The significant decline was confirmed by experiments under controlled ambient CO_2 concentrations (*9*) and could be calibrated against historical CO_2 concentrations inferred from ice cores. An important corollary of this stomatal response to changing CO_2 regimes is that analysis of stomatal frequencies on fossil representatives of extant plant species could help to determine paleoatmospheric CO_2 concentrations at different geologic times. Because of the fossilization potential of the biopolymer cutan (*10*), analysis of fossil leaf cuticles can provide relevant information on stomatal frequencies. Several studies have explored the potential of cuticle analysis in late Pleistocene and Holocene paleoatmospheric research (*11*). In this report, we concentrate on the late Neogene. We based our data on the study of the cuticle of *Quercus petraea* (Durmast oak) from successive time intervals that were characterized by contrasting climatic conditions.

The species *Q. petraea* is essentially European, with a present distribution from southern Scandinavia to the Mediterranean region. The fossil record of this deciduous oak extends back to the late Miocene (*12*). We analyzed leaf compressions (Fig. 1) that were collected from clay intercalations in terrestrial late Miocene and Pliocene sequences of the Lower Rhine Embayment (the current southeastern margin of the Neogene North Sea Basin exposed in Germany and adjacent parts of the Netherlands). Source strata were deposited during five successive, regionally recognized time intervals between ~10 million years ago (Ma) and ~2.5 Ma (*13*), namely, base

---

J. Van Der Burgh, H. Visscher, W. M. Kürschner, Laboratory of Paleobotany and Palynology, Utrecht University, Heidelberglaan 2, 3584 CS Utrecht, the Netherlands.
D. L. Dilcher, Paleobotany Laboratory, Florida Museum of Natural History, University of Florida, Gainesville, FL 32611.

*To whom correspondence should be addressed.